Hardening and Coherent Precipitates Size Evolution with Aging Fe-12Al-12V Alloy

Ferreirós, Pedro; Alonso, Paula R ; Rubiolo, Gerardo H

DOI:
10.1016/j.mspro.2015.04.027

Available online at www.sciencedirect.com

ScienceDirect

Procedia Materials Science 9 (2015) 213 – 220

Procedia Materials Science

www.elsevier.com/locate/procedia

International Congress of Science and Technology of Metallurgy and Materials, SAM – CONAMET 2014

Hardening and coherent precipitates size evolution with aging Fe-12Al-12V alloy

Pedro A. Ferreirós[a,b]*, Paula R. Alonso [a,b], Gerardo H. Rubiolo [a,b,c]

[a]*Instituto Sabato, Universidad de San Martín (UNSAM)-CNEA, Av. General Paz 1499, San Martín B1650KNA, Buenos Aires, Argentina*
[b]*Gerencia deMateriales (GIDAT-CAC), Comisión Nacional de Energía Atómica (CNEA), Av. Gral. Paz 1499, San Martín B1650KNA, Argentina*
[a]*Consejo Nacional de Investigaciones Científicas y Técnicas (CONICET), Av. Rivadavia 1917, C1033AAJ, CABA, Argentina*

Abstract

Fe-Al based alloys have a remarkable potential for high temperature structural applications, provided that the limitation of their low creep resistance is solved. Third element addition (Nb, Ti, Zr or Ta) has proved to perform the task, at the expense of a low ductility. In previous works we have investigated ferritic alloys in the Fe-Al-V system with coherent precipitation of $L2_1$ phase (Fe_2AlV) and have identified phases in equilibrium at the vertical section $Fe_{1-2x}Al_xV_x$. We have found that a wide two-phase field is present in the composition range $0.10 \leq x \leq 0.15$ (x: atomic fraction) till 720 ºC. In this work we study the feasibility of a structural application at high temperatures of the Fe-12Al-12V alloy. We look for ageing conditions leading to a stable coherent precipitation that could strengthen the ferritic matrix. In this way, we measured vickers hardness of coherent $L2_1$ precipitates at 600, 650 and 700 ºC. In all cases hardness has a typical behavior with hardness maximum located at longer times and higher intensities as temperature decreases. We measured size evolution with time through Transmission Electron Microscopy of precipitates at 700 ºC ageing temperature. As a further result, we could calculate from these measurements the activation energy for precipitate growth.

Peer-review under responsibility of the Scientific Committee of SAM–CONAMET 2014

Keywords: Fe-Al-V alloys; Coherent precipitates, Hardening, Aging, Transmission Electron Microscopy

* Corresponding author. Tel.: 054 11 6772 7247; fax: 054 11 6772 7362.
E-mail address: ferreiros@cnea.gov.ar

Peer-review under responsibility of the Scientific Committee of SAM–CONAMET 2014
doi:10.1016/j.mspro.2015.04.027

1. Introduction

Fe-Al based alloys have significant potential for structural applications at elevated temperatures due to their outstanding corrosion resistance at high temperature (Tortorelli and DeVan 1992, Klöwer et al. 1996 and Tortorelli and Natesan 1998) and low density with respect to iron base materials such as micro alloyed or stainless steels. In the same way of comparison, these alloys also offer low cost of raw materials and production processes in conventional mills (McKamey et al. 1996, Stoloff (1998) and Sikka et al. (1998)). Since their melting temperature range goes from about 1200 to 1400 °C, the Fe-Al base alloys can be used for structural applications at temperatures up to 1000 °C. Despite these attractive properties, limited ductility at room temperature (Stoloff and Duquette (1993)) and low creep strength above 600 °C (Morris et al 2006) have hindered wider use of these alloys up to now. The major efforts were focused on improving these properties in single phase iron aluminides (both Fe_3Al ($D0_3$) and FeAl (B2) types) (Palm 2005).

The hardening of the disordered phase α-(Fe, Al) (A2) with coherent precipitates was less attempted. Published reports concerns the deformation behavior at high temperatures of binary Fe-Al alloys containing $D0_3$ phase particles (Morris et al. 1997), ternary Fe-Al-Ni and quaternary Fe-Al-Ni-Cr alloys with B2 phase particles (Stallybrass and Sauthoff 2004, Stallybrass et al. 2005 and Teng et al. 2010) and ternary Fe-Al-Ti alloys with Fe_2AlTi ($L2_1$) particles (Krein et al. 2009). In this context the system Fe-Al-V presents an interesting opportunity. This system was studied because of its outstanding electrical transport properties (Nishino et al. 1997, Hanada et al. 2001 and Vasundhara et al. 2005). The vanadium dilution in Fe_3Al is so high that reaches the Fe_2AlV ($L2_1$) composition and overcomes it. The lattice parameter of the phase $(Fe, V)_3Al$ decreases to a minimum for the composition of the $L2_1$ structure with an approximate value of 0.5761 nm very close to twice the lattice parameter of α-Fe (0.5733 nm). Thus, it might precipitate coherently within the matrix α-(Fe, Al, V). In 1989 it was suggested a ternary Fe-Al-V phase diagram for the iron-rich corner (Zhao et al. 1989). Later the same authors established several phase field boundaries compositions using Transmission Electron Microscopy (TEM) and Energy Dispersive Spectroscopy (EDS) (Maebashi et al. 2004).

Recently, we have studied Fe-Al-V system for the iron-rich corner by computational thermodynamics (Alonso et al. 2011, Ferreirós et al. 2012). We use these theoretical results to search for (A2 + $L2_1$) two phase field alloys with a hardening possibility of the ferrite phase by Fe_2AlV ($L2_1$) coherent precipitation. This search resulted in the establishment of phase equilibria firstly in the selection of the $Fe_{1-2x}Al_xV_x$isopleth of the Fe-Al-V phase equilibrium diagram, and secondly in the experimental determination of the equilibrium phase fields by Differential Scanning Calorimetry (DSC) and TEM techniques (Figure 1) (Ferreirós et al. 2013(a), Ferreirós et al. 2013(b), Ferreirós et al. 2014). Based in those investigations, we could propose that the suitable microstructure for hardness requirement could be found in $Fe_{1-2x}Al_xV_x$alloys with $0.10 \leq x \leq 0.13$ and up to about 720 °C.

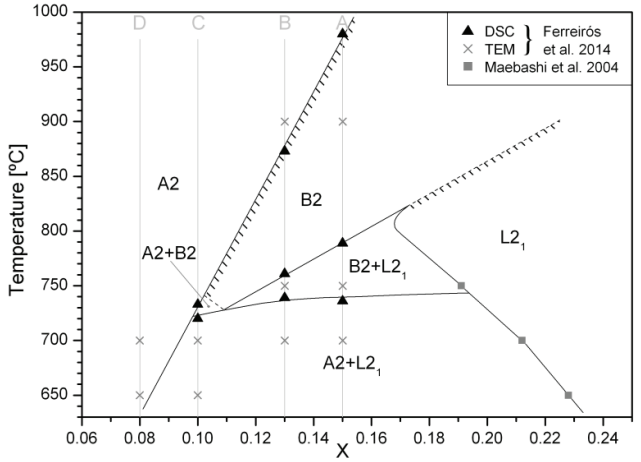

Fig. 1. Section $Fe_{1-2x}Al_xV_x$ of ternary Fe-Al-V phase diagram (Ferreirós et al. 2014).

The desired hardness in these alloys is regulated by the size of coherent precipitates which varies in time according to the temperature used. For this reason, it is essential to understand the mechanisms that control the evolution of the precipitates. Early theories developed on the growth of precipitates were made by Lifshitz and Slyosov (1961) and also by Wagner (1961), from whose work derives its name of "LSW theory". In systems controlled by diffusive mechanisms the LSW theory predicts the growth of the precipitates as the cube of its radius at a constant rate over time (Ardell 1999, Kim and Ardell 2003, Ardell and Ozolins 2005), predicting also precipitate size distributions for cases where the volume fractions are close to zero.

2. Experimental procedure

2.1. Fusion

The alloy was made from 99.97 % iron, 99.99 % aluminum and 99.7 % vanadium. An electric arc furnace with non-consumable tungsten electrode under argon atmosphere and cooper crucible refrigerated by cooled water was used. Previously, to remove oxygen from the furnace chamber, titanium chips were melted. The alloy was remelted four times to ensure chemical homogeneity.

2.2. Hot rolling

As a first step the as cast sample was externally cleaned and polished with emery paper to remove imperfections. After being heated at 1100 °C in an electric furnace with Ar flow, the sample was rolled in several steps without exceeding 10 % reduction in height to a thickness of 3 mm. The roller diameter was 210 mm and a speed of 48 rpm was used.

2.3. Aging heat treatments

Differential scanning calorimeter (DSC) LABSYS evo with Ar flow 25 $mLmin^{-1}$was used for aging heat treatments shorter than 10 hours. Electric resistance furnace was used for longer times than 10 h without inert atmosphere. Samples were fractionated by EDM with copper electrodes. Samples of Ø3x3 mm were used for DSC, and 6x8x3 mm for electric furnace. Thermal treatments performed have two isothermal stages; the first is the solubilization and second is the aging. The decrease in temperature between stages is performed at a rate of 90 $ºCmin^{-1}$ for DSC and 10 $ºCmin^{-1}$ for electric furnace.

2.4. Microscopy

The samples were examined in a Transmission Electron Microscope (TEM) Phillips CM200 with voltage of 160 kV and double tilt sample holder. Thin films were obtained by Electrical Discharge Machining (EDM) cuts, mechanical grinding up to 100 μm and finally electrolytical grinding with a Tenupol-5 Struers, using an electrolyte of 67 % methanol, 33 % nitric acid and temperatures of about -30 °C. Precipitates measurements were performed on TEM images with the Image-Pro Premier program. The amounts of precipitates measured in the micrographs were between 133 and 400 units. The average radius of precipitates was calculated as an average of individual radios from the measured precipitates areas.

2.5. Composition

Measurements of Energy Dispersive Spectroscopy X-ray (EDS) were performed with an EDAX Apollo in a Philips Quanta 200 Scanning Electron Microscope (SEM). To quantify composition, the average of 3 points measurement in remote areas was used.

2.6. Micro hardness

Vickers micro hardness measurements were performed in a Leitz equipment with a 300 g load. The preparation of the measuring surface was performed by mechanical grinding and then polishing with diamond paste till 1 μm.

3. Results and discussion

In a previous work we define the phase equilibrium for the vertical section $Fe_{1-2x}Al_xV_x$ (x: atomic fraction) (Ferreirós et al. 2014). Broad two-phase field (A2 + $L2_1$) was found. Within this field, $L2_1$ spherical precipitates in a ferritic matrix on the maximum coexistence temperature are found for compositions $0.10 \leq x \leq 0.13$ (at higher x, precipitation loses the spherical shape). For this reason, the alloy x = 0.12 (Fe-12% Al-12% V) was selected. Figure 1 shows the phase equilibria for the studied alloy.

Measured EDS compositions on a cross section of the hot rolled alloy are shown in Table 1.

Table 1. EDS compositions.

Elements	Fe	Al	V
Composition (%)	76.21	11.96	11.83
Standard deviation	0.12	0.13	0.02

After hot rolling, aging heat treatments at different times and temperatures of 600, 650 and 700 ºC were performed. Before each aging, solubilization treatment at 900 °C for 10 minutes was performed. In the solubilization the alloy passes completely an A2 phase; then the temperature is reduced to the value chosen for aging and the coherent $L2_1$ phase precipitated and grows.

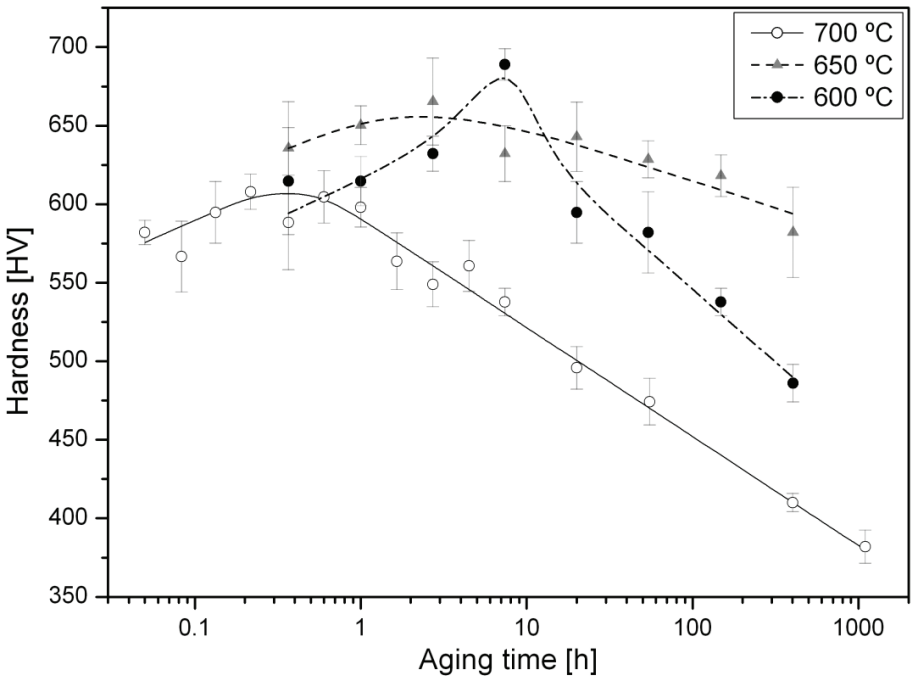

Fig. 2. Hardness as function of aging treatment.

In Figure 2 microhardness measurements versus time for 3 aging treatment temperatures are plotted. It can be seen that the function passes through a maximum hardness; and this maximum shifts to longer times on reducing aging temperature. This behavior where a maximum hardening is obtained is well known and is primarily due to temporal size growth of precipitates while the ratio between matrix volume and precipitates volume remains constant; therefore, precipitates growth is achieved at the expense of the number of precipitates. The maximum hardness is the result of the competition of two displacement dislocation mechanism. These are the cut of precipitate by dislocation and the by-passing of the precipitate by Orowan mechanism (Nembath and Neite 1985). It can be deduced from this analysis that maximum hardness peak obtained at different temperatures corresponds to the same precipitate size, for a given alloy, with constants volume fraction, spherical morphology, and homogeneously dispersed distribution.

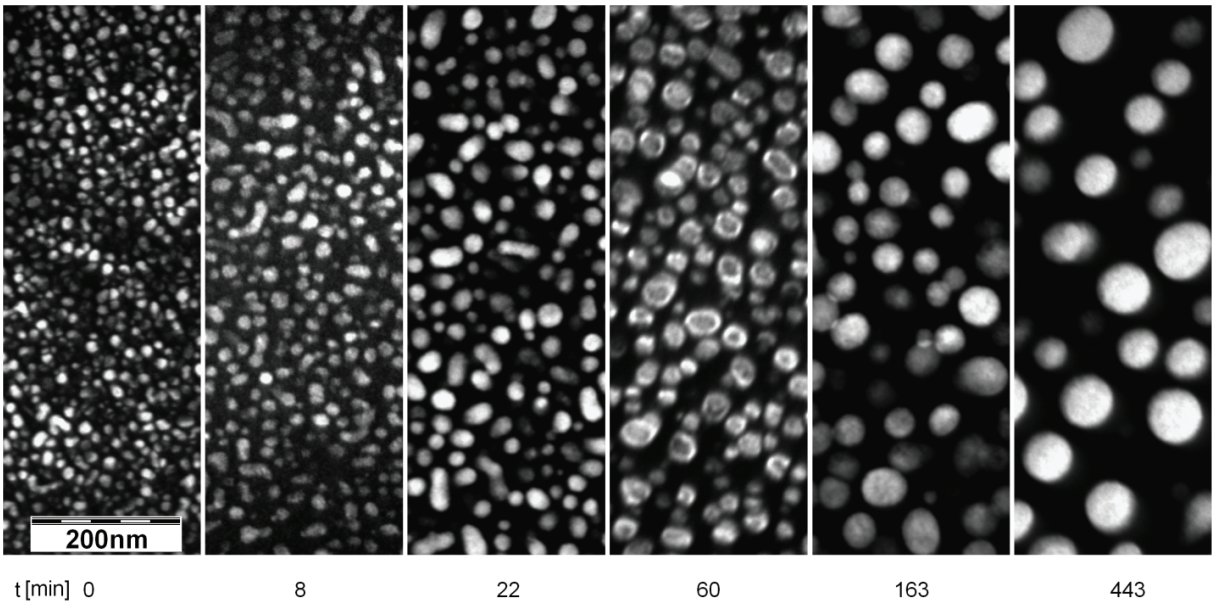

Fig. 3. $L2_1$ coherent precipitates observed in dark field TEM. Samples aged in DSC at 700 °C and different times.

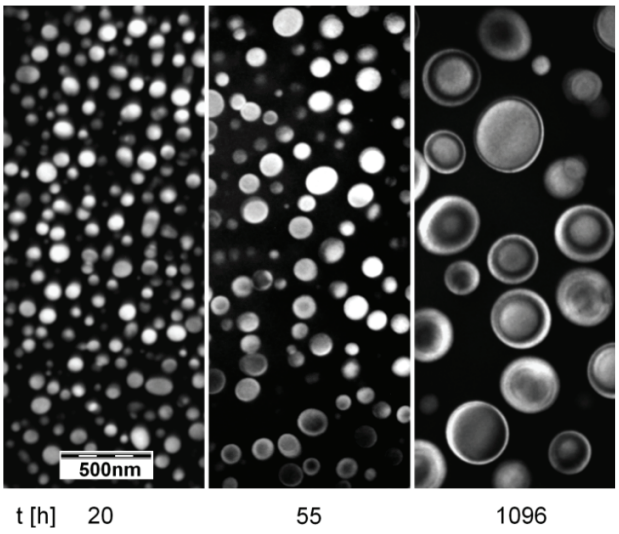

Fig. 4. $L2_1$ coherent precipitates observed in dark field TEM. Samples aged in furnace at 700 °C and different times.

Figure 2 shows that by lowering the temperature of aging treatment, the hardness maximum peak moves to longer times and increases its value. This increment in hardness peak is a known feature (Shewmon 1969). According to our speculation written above, it occurs at constants volume fraction, precipitate size and morphology. The justification for these results can be found by considering that precipitate size dispersions are usually reduced with diminishing temperatures of aging treatments. Although the effect of distribution on the hardness was early analyzed by Munjal and Ardell (1976) with the conclusion that it was not relevant, later other authors (Glazer and Morris 1988) reviewed the literature and showed in a new analysis that a lower dispersion of precipitate size corresponds to a higher intensity hardness peak.

The precipitate sizes resulting of aging at 700ºC and different times were analyzed by TEM. Figures 3 and 4 show micrographs taken with TEM dark fields for some of the aging processes performed. The indicated 0 min aging, corresponds to samples cooled from the 900 °C solubilization temperature to room temperature. The average precipitates radius corresponding to the hardness peak (700 ºC and 0.37 h, Figure 2) is 11.02 nm.

The Figure 5 shows the evolution of the precipitate radius versus aging time for 700 ºC. The error bars in the graph represent the standard dispersions of the precipitates radii. The estimated error in radii measurements was ± 4 nm. The LSW theory of precipitates growth controlled by diffusion, predicts the following relationship for the radius of the precipitate as a function of aging time;

$$\bar{r}^{3}_{(t)} - \bar{r}^{3}_{(0)} = K\,t \tag{1}$$

where r is the radius of precipitates at a given time t, $r_{(0)}$ is the radius at time zero and *K* is a kinetic constant that depends on temperature.

By representing the radius function of time on a logarithmic scale, Eq. (1) predicts a linear response with a slope of 1/3. This slope value is very close to that obtained by the method of least squares (0.31) in Figure 5.

It was assumed above that the peaks of maximum hardness obtained at different temperatures correspond to the same size of precipitate, thus from the Eq. (1) it follows:

$$\bar{r}^{3}_{(t_i^p)} - \bar{r}^{3}_{(0)} = K_i\,t_i^p = \bar{r}^{3}_{(t_j^p)} - \bar{r}^{3}_{(0)} = K_j\,t_j^p \tag{2}$$

where index p indicates the times at which the maximum hardness (peak) are reached and the indices *i*, *j* are two conditions of different treatment temperatures. That is, the product of the constant *K* at each temperature by the time for which the maximum hardness is achieved should be a constant. Moreover, in the LSW theory it is considered that the constant K has a temperature (*T*) dependence with a given Arrhenius activation energy (*Q*), so that energy can be calculated from Eq. (2) as;

$$Q = R\left(\frac{T_i T_j}{T_j - T_i}\right)\ln\left(\frac{t_i^p}{t_j^p}\right) \tag{3}$$

where *R* is the gas constant.

Table 2.Heat treatment conditions for maximum aging precipitation hardening.

T (K)	t_p(h)
973	0.37
923	2.72
873	7.38

Applying Eq. (3) at three possible combinations between the temperatures of 600, 650 and 700 ºC gives three activation energies and their average is Q = 214 kJmol^{-1}. The values of temperature and time of hardness peak

applied in Eq. (3) for calculating Q, are shown in Table 2. The result obtained for the activation energy is close to experimental values measured by diffusion on a ferritic matrix, for the three pure elements in this alloy (Table 3).

Table 3. Activation energies (Q) for elements diffusion in α-Fe. Temperatures indicate the range of experimental measurement (Landolt-Börnstein 1990).

Element	T (K)	Q (kJmol^{-1})
Fe	973	271
Al	1003-1673	228
V	1058-1172	274

4. Conclusion

We verified a good agreement between the temporal evolution at 700 ºC of the average size of coherent precipitates $L2_1$ on a α-Fe matrix in the Fe-12%Al-12%V (at%) alloy with the LSW theory predictions. For aging times such that $0 \leq t \leq 1096$h precipitates showed a spherical morphology.

The maximum hardness of the alloy was obtained for 11.02 nm precipitate average radii, which corresponds to aging treatments of 600, 650 and 700 ºC for 7.38 h, 0.37 h and 2.72 h respectively.

Activation energy resulting for the precipitates growth was Q = 214 kJmol^{-1}.

Acknowledgements

We thank the groups directed by Drs. S.F. Aricó, M.J. Iribarren, and P.B. Bozzano, pertaining to the Gerencia Materiales of CNEA-CAC, the availability of equipment that allowed us to perform this research.This work was performed in the Departamento Transformaciones y Propiedades of Gerencia Materiales, CAC – CNEA.

References

Alonso P.R., Gargano P.H., Bozzano P.B., Ramírez-Caballero G.E., Balbuena P.B., Rubiolo G.H., 2011. Combined ab initio and experimental study of A2+$L2_1$ coherent equilibria in the Fe-Al-X (X = Ti, Nb, V) systems. Intermetallics 19, 1157–67.

Ardell A.J., 1999. Microstructural stability at elevated temperatures. J. Eur. Ceram. Soc. 19, 2217-31.

Ardell A.J., Ozolins V., 2005. Trans-interface diffusion-controlled coarsening. Nature Materials 4, 309-16.

Ferreirós P.A., Alonso P.R., Gargano P.H., Bozzano P.B., Troiani H.E., Rubiolo G.H., 2013(a). Transformaciones de fase en aleaciones $Fe_{1-2x}Al_xV_x$ (X≤0,15). Anales SAM/CONAMET, T4C.3

Ferreirós P.A., Alonso P.R., Baruj A., Rubiolo G.H., 2013(b). Endurecimiento por precipitación coherente de la fase Fe_2AlV en aleaciones $Fe_{1-2x}Al_xV_x$. Anales SAM/CONAMET, T4C.1

Ferreirós P.A., Alonso P.R., Gargano P.H., Bozzano P.B., Troiani H.E., Baruj A., Rubiolo G.H., 2014. Characterization of microstructures and age hardening of $Fe_{1-2x}Al_xV_x$ alloys. Intermetallics 50, 65–78.

Ferreirós P.A., Gargano P.H., Alonso P.R., Rubiolo G.H., 2012. Equilibrio coherente $L2_1$+A2 en el sistema Fe-Al-V. Anales SAM/CONAMET, 2.415

Glazer J., Morris Jr. J.W., 1988. The effect of the precipitate size distributions on the aging curve of order hardening alloys. Acta Metall. 36, 907-15.

Hanada Y., Suzuki R.O., Ono K., 2001. Seebeck coefficient of $(Fe,V)_3Al$ alloys. J. Alloys Compounds 329, 63-8.

Kim D.M., Ardell A.J., 2003. Coarsening of Ni_3Ge in binary Ni–Ge alloys: microstructures and volume fraction dependence of kinetics. Acta Mater. 51, 4073-82.

Klöwer J., 1996. High temperature Corrosion behaviour of iron aluminides and iron-aluminium-chromium alloys. Mater. Corros. 47, 685–94.

Krein R., Palm M., Heilmaier M., 2009. Characterization of microstructures, mechanical properties, and oxidation behaviour of coherent A2+$L2_1$ Fe–Al–Ti alloys. J. Mater. Res. 24, 3412–21.

Landolt-Börnstein, Numerical Data and Functional Relationships in Science and Technology, 1990. Diffusion in solid Metals and Alloys. Vol. 26. Springer-Verlag, Berlín.

Lifshitz I.M., Slyosov V.V., 1961. The kinetics of precipitation from supersaturated solid solutions. J. Phys. Chem. Solids, 19, 35-50.

Maebashi T., Kozakai T., Doi M., 2004. Phase equilibria in iron-rich Fe-Al-V ternary alloy system. Z. Metallkd. 95, 1005–10.

McKamey C.G., 1996. “Physical metallurgy and processing of intermetallic compounds”. In: Stoloff N.S., Sikka V.K., (Ed.). Chapman and Hall, New York, pp. 351.

Morris D.G., Gunther S., 1997. Room and high temperature mechanical behaviour of a Fe_3Al-based alloy with α-α' microstructure. Acta Materialia 45, 811–22.

Morris D.G., Muñoz-Morris M.A., Requejo L.M., Baudin C., 2006. Strengthening at high temperatures by precipitates in Fe–Al–Nb alloys. Intermetallics 14, 1204–07.

Munjal V., Ardell A.J., 1976. The effect of particle size distributions on the CRSS of aged Ni-Al alloys. Acta Metall. 24, 827-33.

Nembach G., Neite G., 1985. Precipitation hardening of superalloys by ordered γ′-particles. E. Progress in materials Science 29, 177-319.

Nishino Y., Kato M., Asano S., Soda K., Hayasaki M., Mizutani U., 1997. Semiconductor like Behavior of Electrical Resistivity in Heusler-type Fe_2VAl. Phys. Rev. Letter 79, 1909–12.

Palm M., 2005. Concepts derived from phase diagram studies for the strengthening of Fe-Al-based alloys. Intermetallics 13, 1286–95.

Shewmon P.G., 1969. Transformations in Metals, McGraw Hill Book Company, New York, pp. 286.

Sikka V.K., Wilkening D., Liebetrau J., Mackey B., 1998. Melting and casting of FeAl-based cast alloy. Mater Sci Eng A 258, 229–35.

Stallybrass C., Sauthoff G., 2004. Ferritic Fe–Al–Ni–Cr alloys with coherent precipitates for high-temperature applications. Mater Sci Eng A 387, 985–90.

Stallybrass C., Schneider A., Sauthoff G., 2005. The strengthening effect of (Ni, Fe)Al precipitates on the mechanical properties at high temp. of ferritic Fe–Al–Ni–Cr alloys. Intermetallics 13, 1263–68.

Stoloff N.S., 1998. Iron aluminides: present status and future prospects. Mater Sci Eng A 258, 1-14.

Stoloff N.S., Duquette D.J., 1993. Moisture and hydrogen-induced embrittlement of iron aluminides. JOM 45, 30–4.

Teng Z.K., Liu C.T., Ghosh G., Liaw P.K., Fine M.E., 2010. Effects of Al on the microstructure and ductility of NiAl-strengthened ferriticsteelsat room temp. Intermetallics 18, 1437–43.

Tortorelli P.F., DeVan J.H., 1992. Behavior of iron aluminides in oxidizing and oxidizing/sulfidizing environments. Mater Sci Eng A 153, 573-77.

Tortorelli P.F., Natesan K., 1998. Critical factors affecting the high-temperature corrosion performance of iron aluminides. Mater Sci Eng A 258, 115–25.

Vasundhara M., Srinivas V., Rao V.V., 2005. Low-temperature electrical transport in Heusler-type $Fe_2V(AlSi)$ alloys. Journal of Physics: Condensed Matter 17, 6025–36.

WagnerC., 1961. Theorie der Alterung von NiederschlägendurchUmlösen (Ostwald-Reifung).Z. Electrochem 65, 581-91.

Zhao P.Z., Kozakai T., Miyazaki T., 1989. Phase Separations into A2+ DO_3 Two Phases in Fe-Al-V Ternary Ordering Alloys. J. Japan Inst.Metals 53, 266–72.